Interstitial Fe in Si and its interactions with hydrogen and shallow dopants

M. Sanati, N. Gonzalez Szwacki, and S. K. Estreicher*
Physics Department, Texas Tech University, Lubbock Texas 79409-1051, USA
(Received 19 March 2007; revised manuscript received 20 June 2007; published 11 September 2007)

The properties of interstitial iron in crystalline silicon and its interactions with hydrogen, shallow acceptors (B, Al, Ga, In, and Tl), and shallow donors (P and As) are calculated from first-principles in periodic supercells. The interactions between the {Fe,B} pair and interstitial hydrogen are also examined. The configurations, electronic structures, and binding energies are predicted. The relative stability of the trigonal and orthorhombic structures of the Fe-acceptor pairs are calculated as a function of charge state and temperature. The gap levels are estimated using the marker method. The vibrational spectra of the complexes containing light impurities (H or B) are predicted.

DOI: 10.1103/PhysRevB.76.125204 PACS number(s): 63.20.Mt, 61.72.Bb

I. INTRODUCTION

Transition metal (TM) impurities are common and most often undesirable contaminants in both integrated-circuit grade Si and Si-based photovoltaic materials. Istratov, Hieslmair, and Weber have reviewed the properties of Fe and its complexes in Si (Ref. 1) as well as the possible sources of Fe contamination.[2] These reviews underscore how little is known at the atomic level about the chemistry of Fe in Si.

Some Fe is always present in the source material. Its solubility sharply decreases as the sample cools down from the melting point to room temperature. Thus, the as-grown crystal is often supersaturated with Fe. Interstitial iron (Fe_i) readily diffuses and traps within hours at shallow acceptors or TMs, precipitates a various defects including oxides, and may even form silicides. Many of these defects are magnetically and electrically active.

More than thirty Fe-related complexes have been detected by electron paramagnetic resonance (EPR), electron-nuclear double resonance (ENDOR), deep-level transient spectroscopy (DLTS) or other experimental techniques. In some cases, a specific center has been identified. In many cases, the structure of the defect is not conclusively known. A summary of the key results relevant to the present work is as follows.

EPR,[3] ENDOR,[4] and Mössbauer studies[5,6] show that Fe_i resides at the tetrahedral interstitial (T) site. The fitting of β^- channeling patterns[7] following the implantation of the radioactive isotope ^{59}Fe implies that Fe becomes substitutional following high-temperature (above 800 °C) anneals. At lower temperatures, Fe is near T site, where "near" means 0.3–0.8 Å. Such a large displacement and the associated symmetry lowering relative to the T site is not observed in the EPR and ENDOR data. It is possible that the defect centers formed in the channeling experiments involve native defects.

The diffusivity of Fe_i has been measured by a number of groups using a range of experimental methods. The activation energies[1] span the range 0.49–0.92 eV. The charge state of the diffusing species is not always known with certainty and trap-limited diffusion could affect some measurements. A fit to all the data over a wide range of temperatures leads[1] to the activation energy for diffusion ~0.67 eV. Several authors[8,9] find that the activation energy for diffusion of Fe_i^+ (~0.69 eV) is lower than that of Fe_i^0 (~0.84 eV). These values have been debated.[10,11] Measurements of the formation rates of Fe-acceptor pairs show that the pairing kinetics are largely independent of the dopant and involve[12] an activation energy in the range 0.66–0.68 eV, suggesting that the process is limited by the diffusion of Fe_i^+.

Hall effect and resistivity measurements[13,14] show the existence of a donor level of Fe_i, but iron contamination of n-type Si does not reduce the concentration of free electrons, suggesting that the isolated interstitial has no deep acceptor level. The position of the (0/+) level has been measured to be in the range 0.39–0.45 eV (Ref. 1) from photoionization,[15,16] DLTS,[14,17–20] and the monitoring of the EPR intensities of Fe_i^+ and Fe_i^0 as a function of the Fermi level.[21] The latter work confirms that only Fe_i^+ and Fe_i^0 exist for Fermi levels in the range $E_v+0.045$ eV to $E_c-0.045$ eV.

Ludwig and Woodbury[22] and Feher[23] have proposed a model for the electronic structure of 3d TM impurities in the Si crystal field. The (atomic) 4s electrons are transferred to the 3d shell. In tetrahedral symmetry, these electrons populate a t_2 and an e levels (the latter is slightly higher in energy) in accordance with Hund's rule. In the case of Fe_i^0 for example, the $4s^23d^6$ atomic structure becomes $4s^03d^8$, the eight electrons populate the t_2 and e levels, and Fe_i^0 has spin 1. Similarly, Fe_i^+ has spin $\frac{3}{2}$. These spin states are consistent with the EPR data. Note that since the e level is above the t_2 level, Fe_i^+ is an orbital triplet and a Jahn-Teller distortion should result. The EPR lines associated with Fe_i^+ are much broader than those associated with Fe_i^0. This could be consistent with a dynamic Jahn-Teller effect.[24,25]

In p-type material, Fe_i^+ readily interacts with (ionized) shallow acceptors. The trigonal (C_{3v}) {Fe,B} pair was first observed by EPR,[26,27] then ENDOR.[28] It is a strong recombination center with a donor level near $E_v+0.11$ eV (Refs. 14 and 29–34) and a deep acceptor level near $E_c-0.29$ eV.[20,30,34] These values have recently been confirmed by temperature-dependent and injection-dependent lifetime spectroscopy data.[35] A second acceptor level at $E_v+0.074$ eV (Refs. 32 and 33) is tentatively associated with a metastable orthorhombic (C_{2v}) configuration of the pair. Under minority carrier injection, the amplitude of the $E_c-0.29$ eV signal diminishes as a new level at $E_c-0.43$ eV

appears, suggesting that this is the acceptor level of the {Fe,B} pair in the orthorhombic configuration.[33] The binding energy E_b, defined from $Fe_i^+ + B^- \rightarrow \{Fe,B\}^0 + E_b$, is in the range 0.58 eV (Refs. 36–38) to 0.65 eV.[20,39] Photoluminescence (PL) studies[40] show the existence of optically-active defects which incorporate B and Fe but are distinct from the {Fe,B} pair discussed here.

The neutral charge state of the {Fe,Al} pair has been detected by EPR in a trigonal (stable) and an orthorhombic (metastable) configuration,[41,42] with spin $\frac{3}{2}$.[42,43] The positive and negative charge states of the trigonal configuration have also been detected.[43–45] In the dark, the thermally induced activation energies for reorientation[46] are 0.5 eV for $\langle 100\rangle \rightarrow \langle 111\rangle$ and 0.6 eV for $\langle 111\rangle \rightarrow \langle 100\rangle$. One would expect such numbers were Fe to simply hop from the second-nearest to the nearest T site to the acceptor and vice versa. Under illumination, these activation energies drop to ~0.1 eV.[47] Following in-diffusion, cooling the sample under illumination produces both DLTS signals, while cooling in the dark enhances the trigonal signal.[46] The binding energy in the trigonal configuration is in the range 0.52 (Ref. 46) to 0.70 eV (Ref. 38) and the donor levels[46] are at $E_v+0.20$ eV (C_{3v}) and $E_v+0.13$ eV (C_{2v}).

The neutral charge state of the {Fe,Ga} pair has been detected by EPR (Refs. 26, 42, 48, and 49) in both the trigonal (stable) and orthorhombic (metastable) configurations with spin $\frac{3}{2}$. The donor levels are at $E_v+0.24$ eV (C_{3v}) (Refs. 14, 38, and 50) and $E_v+0.14$ eV (C_{2v}).[51] The binding energy in the trigonal configuration is $E_b=0.47$ eV.[38]

The EPR signal of the neutral {Fe,In} pair was detected in the stable C_{2v} (Refs. 26, 52, and 53) and the metastable C_{3v} (Refs. 54 and 55) configurations. The latter was achieved following illumination of the sample with 0.5 eV photons. The positive charge state of the pair has also been observed.[52,56] DLTS studies[51] show donor levels at $E_v+0.15$ eV in the orthorhombic and $E_v+0.27$ eV in the trigonal configurations. Fourier transform infrared absorption (FTIR) experiments[57–59] of the excitation spectrum of {Fe,In} find the acceptor levels at $E_c-0.39$ eV (C_{2v}) and $E_c-0.32$ eV (C_{3v}).

Finally, the existence of a metastable complex involving Fe and Tl has been inferred from PL bands.[60] The trigonal symmetry proposed by Sauer and Weber[61] was later confirmed.[62,63] The intensities of the PL bands increases with the Fe_i concentration. However, the identification of these PL bands with {Fe,Tl} pairs has yet to be confirmed.[1,64]

Thus, each Fe-acceptor pair has two configurations with three possible charge states as well as a donor and an acceptor level in each of them. The Fe pair with B, Al, and Ga is stable in the C_{3v} configuration, with Fe at the nearest T site to the acceptor. In the case of Al and Ga, the C_{2v} configuration with Fe at the second-nearest T site is energetically very close. As for {Fe,In}, the C_{2v} configuration has the lowest energy.

Chantre *et al.*[46,51] have used the ratios of the DLTS intensities for various biases during cool down to estimate the relative populations of the trigonal and orthorhombic configurations, and then fit them to a Boltzmann term. The energy differences ΔE they obtained in the 0 and + charge states are $\Delta E(0)=0.14, 0.13, -0.01$ eV and $\Delta E(+)=0.07, 0.03, -0.13$ eV for Al, Ga, and In, respectively. A positive value favors the trigonal configuration. These small energy differences have been compared to various potential energy predictions (see Ref. 1). However, the measured ΔE's are not true $T=0$ K potential energy differences, but rather the differences between free energy minima at the temperature T_{min} below which Fe_i is not longer able to overcome the energy barrier (~0.5–0.6 eV) between the two sites in the time scale commensurate with the cooling down rate.

There is no direct evidence for the existence of Fe-donor pairs. A decrease in the Fe_i^0 signal with increasing P_s^+ concentration has been interpreted as evidence of Fe-P pairing[65] with a binding energy of 0.9 eV. However, no change in the EPR spectrum of phosphorus has been observed even after the Fe_i^0 signal disappears following long 200 °C anneals.[66] Four weak satellites in the EPR spectrum of Fe_i^0 at high P or As concentrations exist, but they are weaker than would be expected for close pairs. The formation of $Fe_i^{--}P_s^+$ pairs has been proposed[67] but there is no experimental or theoretical evidence of even a single acceptor level of Fe_i in the gap. An EPR-active {Fe,P} pair has been detected in irradiated n-type Si, but this complex most probably involves one or more vacancies.[68]

Sadoh *et al.*[69] performed thermally stimulated capacitance and DLTS measurements in n-type Si samples contaminated with Fe and subsequently etched with H-containing chemicals. The presence of a C-H complex confirmed that H penetrated into the sample. In addition to the Fe_i donor level observed at $E_v+0.41$ eV, the authors tentatively assigned a new donor level at $E_v+0.31$ eV to a $\{Fe_iH\}$ pair. This signal disappears after annealing at 175 °C for 30 min.

The early theoretical work on interstitial 3d TM impurities in Si has focused on explaining trends in the electronic structure and gap levels using methods that do not allow for defect geometries to be optimized. Since Fe_i is known to have tetrahedral symmetry, it was assumed that the impurity resides at an undisturbed T site. Our geometry optimizations (see below) show that this assumption is valid. The scattering $X\alpha$ method in H-terminated clusters,[70] later enhanced with semi-empirical Hartree-Fock calculations,[71] have been successful at predicting many qualitative features of these impurities. They predicted the donor level of Fe_i to be at $E_v+0.68$ eV.

Zunger and co-workers[72–76] used a self-consistent local density functional (LDF) Green's function scheme to study trends and predicted the spin-polarized electronic structure of Fe_i.[74] They found its donor level to be at $E_v+0.53$ eV (Ref. 72) or $E_v+0.32$ eV.[74,75] Beeler *et al.*[77] performed calculations within the spin-unrestricted LDF linear muffin-tin-orbital Green's function method. They predict a spin $\frac{3}{2}$ for Fe_i^+ and a spin 1 for Fe_i^0, in agreement with experiment. They also predict the donor level of Fe_i to be at $E_v+0.25$ eV, close to the DLTS value.

Weihrich and Overhof[25] have calculated in detail the electronic structure and hyperfine parameters of Fe_i in the + and 0 charge states, using a Dyson's equation approach to solve the Kohn-Sham equation within local spin-density-functional theory and calculated the Green's function within a linear

muffin-tin approach using the atomic-spheres approximation. These calculations do not allow geometry optimizations to be performed. The authors predict the donor level of Fe_i to be at $E_v+0.29$ eV.

The interactions between Fe and shallow dopants have been discussed by several authors. Assali and Leite[78] use the scattering $X\alpha$ method in small hydrogen-saturated clusters to calculate the electronic structure of the C_{3v} {Fe,B} pair, without spin polarization. They predict a strongly covalent Fe-B interaction. Sugimoto and Seki[79] used H-terminated clusters within unrestricted *ab initio* Hartree-Fock theory, with a combination of minimal and double-zeta basis sets. The acceptor atoms (B, Al, Ga, and In) were assumed to be at unrelaxed substitutional sites. The authors find the C_{3v} configuration to be more stable for B, Al, and Ga, but the C_{2v} one is more stable in the case of In. The population analysis of the {Fe,B} pair shows that Fe_i overlaps only very weakly with B, which argues against the mostly covalent character predicted in Ref. 78.

Overhof and Weihrich[67] used their Green's function approach[25] (without lattice relaxations) to study the trigonal and orthorhombic configurations of the Fe-acceptor pairs. Their calculations predict a mostly ionic bonding between Fe and the acceptors. Their calculated binding energies are 0.78 eV for {Fe,B} and 0.28 eV for {Fe,Al}. They also calculate the relative energies between the two configurations, but the predictions are affected by the absence of geometry optimization. The calculated donor and acceptor levels for the Fe-acceptor pairs are in reasonable agreement with experiment. The authors also predict a pairing between Fe_i^{--} and P_s^+.

Zhao *et al.*[80] used an ionic model with elastic and electrostatic interactions to show that the driving force for the Fe_i^+-A_s^- pairing is electrostatic. They also calculated trends in the position of the donor level and the relative energies of the C_{3v} and C_{2v} configurations.

The present work differs from the previous theoretical approaches in several ways. First, the host crystal is represented by 64 to 216 atoms periodic supercells. These are not as ideal a representation of the isolated impurity in an otherwise perfect crystal as that provided by Green's functions, but they allow the use of conjugate gradient geometry optimizations. Second, we use a first-principles spin-density-functional approach within the generalized gradient approximation (GGA), with both plane-wave and pseudoatomic basis sets for the single particle states.

Such a "first-principles" theoretical approach has been successfully used to study a wide range of defects, impurities, pairs, and small complexes in Si and numerous other host crystals.[81] In this paper, we focus on the properties of Fe_i, including its interactions with interstitial H, and Fe pairs with shallow substitutional dopants B, Al, Ga, In, Tl, P, and As. The possibility of interactions between the {Fe,B} pair and interstitial H is also investigated. The geometries, electronic structures, and spin states are calculated for all the possible charge states of the defects. The binding energies of the complexes are predicted. The existence and approximate location of donor and acceptor levels are obtained using the marker method.[82] The vibrational spectra of the complexes containing light impurities are calculated as well.

Note that detailed first-principles calculations of the hyperfine parameters of Fe_i in the + and 0 charge states and iron-acceptor pairs have been successfully performed.[25,67] In situations were the impurity can be assume to reside at undistorted high-symmetry sites—as is the case here (see below)—these calculations are better suited than our pseudopotential method to reproduce the EPR and ENDOR data. We do not focus on this aspect of the problem.

Section II discusses the methodology. Section III contains the results for Fe_i and its interactions with H. Section IV deals with Fe pairs with shallow acceptors (B, Al, Ge, In, Tl) and donors (P, As). We also consider the possibility that the {Fe,B} pair interacts with interstitial H. A summary and a discussion are in Sec. V. The interactions of Fe with native defects and other common impurities will be the subject of a later paper.

II. METHODOLOGY

The present calculations are carried out using two first-principles spin-density-functional packages, VASP (Refs. 83–86) and SIESTA (Refs. 87 and 88), within GGA to the exchange-correlation potential (see Ref. 89 for VASP and[90] for SIESTA). The reason for repeating a number of calculations with a plane-wave and a local basis set code is to make sure that the predictions are independent of the choice of basis set and pseudopotential. Although convergence is sometimes more difficult to achieve with SIESTA than VASP, the structures, energy differences between configurations or spin states, vibrational spectra, and even thermodynamic gap levels calculated with both codes are in close agreement with each other and, when available, with experiment. Any substantial discrepancy is noted in the text. The binding energies listed in the text have been obtained with VASP, the vibrational spectra with SIESTA, and gap levels are calculated using projector augmented-wave (PAW) potentials[91] as implemented in VASP. We denote the spin and charge state of a defect X as ${}^{\text{spin}}X^{\text{charge}}$.

In most of our calculations, the host crystal is represented by a 64 host atoms periodic supercell. We also use the 128 and 216 host atoms cells in situations where size effects are expected to be significant, that is when calculating the binding energies of Fe-acceptor pairs. The lattice constant of all the cells is optimized. A $2\times2\times2$ Monkhorst-Pack[92] mesh is used to sample the Brillouin zone for all the calculations except dynamical matrices and gap levels (see below). The defect geometries are optimized with a conjugate gradient algorithm.

The VASP calculations use plane-wave basis set and ultrasoft Vanderbilt type pseudopotentials.[93] In the VASP approach, the solution of the self-consistent Kohn-Sham equations are obtained using an efficient matrix-diagonalization routine based on sequential band-by-band residual minimization method and Pulay-like charge density mixing.[94] A plane-wave basis cutoff of 321 eV is used for the ultra-soft pseudopotential calculations. With PAW potentials, the cutoff is 398 eV.

The SIESTA calculations use norm-conserving pseudopotentials in the Troullier-Martins form[95] to remove the core

regions from the calculations. The basis sets for the valence states are linear combinations of numerical atomic orbitals.[87,96,97] In the present calculations, we use double-zeta basis sets (two sets of valence s and p's) for the first and second-row elements (H and B), and double-zeta polarized basis sets (two sets of valence s and p's plus one set of d's) for elements on the third row and below. The charge density is projected on a real-space grid with an equivalent cutoff of 250 Ryd to calculate the exchange-correlation and Hartree potentials. This large cutoff is needed to describe the localized d states of iron.

The ultrasoft and PAW pseudopotentials are part of the VASP package. The SIESTA Fe pseudopotential has been optimized by Izquierdo *et al.*[98,99] It includes nonlinear core corrections. We use the same orbital populations in VASP as in SIESTA. The SIESTA pseudopotential for other elements have been optimized using the experimental bulk properties of the perfect solids and/or first-principles calculations[100] as well as vibrational properties of appropriate free molecules or defects when experimental data are available. This testing leads to a fine-tuning of the pseudopotential parameters relative to the purely atomic ones: small changes in the core radius and/or orbital populations. Once optimized, we take these pseudopotentials to be transferable to the defect problems at hand. For the heavy elements (Ga, In, Tl), the semicore d electrons are always included in the valence states.

The dynamical matrices are calculated using the force-constant method with k-point sampling restricted to the Γ point. Their eigenvalues are the normal-mode frequencies ω_s. The orthonormal eigenvectors $e^s_{\alpha i}$ $(i=x,y,z)$ give the relative displacements of the nuclei α for each mode s. A quantitative measure of how localized a specific mode is on one atom or a group of atoms is provided by a plot of $L^2_{\{\alpha\}}=(e^s_{\alpha x})^2+(e^s_{\alpha y})^2+(e^s_{\alpha z})^2$ vs s or ω_s. Here, $\{\alpha\}$ may be a single atom (e.g., Fe) or a sum over a group of atoms [e.g., the Si nearest neighbors (NNs) to Fe]. Such a *localization plot* allows the identification of all the local and pseudolocal[101] vibrational modes in the cell (LVMs and pLVMs, respectively) as well as the resonant modes associated with a specific defect. The knowledge of all the normal modes also allows the construction of the phonon density of states $g(\omega)$. We obtain this function by evaluating the dynamical matrix at 100 k points in the Brillouin zone of the supercell. Once $g(\omega)$ is known, the Helmholtz vibrational free energy F_{vib} is straightforward to calculate.[102]

The gap levels are estimated using the marker method.[82] The calculated ionization energies and electron affinities are scaled to a known marker which we take to be the perfect crystal. The same scaling is used to determine the donor and acceptor levels of the defect. We choose the perfect crystal as a reference point because there is no single marker that could be considered ideal for all the defects studied in the paper. Further, the geometry optimizations show that no substantial distortion is involved. Our best estimates for the gap levels are obtained with PAW (Ref. 91) potentials[86] with a $3\times3\times3$ k-point sampling. The $3\times3\times3$ SIESTA values are given in some cases for comparison. The PAW potentials are more accurate than the ultrasoft ones because the radial cutoffs (core radii) are smaller and the PAW potentials reconstruct the exact valence wave function with all nodes in the core region. The PAW method gives energy differences very close to the ones obtained with the best full-potential linearized augmented-plane-wave method.

III. RESULTS

A. Fe_i and $\{Fe_iH\}$

As expected, we find that Fe_i resides at an undistorted T site in both the + and 0 charge states, with spin $\frac{3}{2}$ and 1, respectively. No Jahn-Teller distortion is apparent in our calculations, which is not surprising at this level of theory. The spin 0 and 2 states of Fe_i^0 are 0.74 and 0.69 eV higher than the spin 1 state, respectively. The spin $\frac{1}{2}$ state of Fe_i^+ is 0.30 eV above the spin $\frac{3}{2}$ state. We find a donor level in the gap at $E_v+0.28$ eV (SIESTA: 0.37 eV), but no acceptor level.

A population analysis of $^{3/2}Fe_i^+$ shows that the impurity does weakly overlap with its Si neighbors. The overlap populations with each of the four NNs and the six second-NNs are 0.17 and 0.12, respectively. These numbers are small but positive. The spin population in the valence orbitals is 0.016 in the $4s$, 0.024 in the $4p$, and 1.140 in the $3d$ states. Thus, 78% of the total spin is localized on $^{3/2}Fe_i^+$, and the rest is on the neighboring Si atoms. In the case of $^1Fe_i^0$, the overlap populations are almost the same (0.17 and 0.13, respectively) but the spin populations are 0.013, 0.016, and 0.964, respectively. Thus, over 96% of the spin resides on $^1Fe_i^0$.

The activation energies for diffusion of $^{3/2}Fe_i^+$ and $^1Fe_i^0$ along T-hexagonal-T sites are 0.69 and 0.76 eV, respectively. We obtained these values by placing Fe at the hexagonal interstitial site with both an unrelaxed crystal and a fully relaxed one. The former provides an upper bound for the activation energy (0.92 and 0.91 eV in the + and 0 charge states, respectively) and the latter a lower bound (0.47 and 0.60 eV in the + and 0 charge states, respectively). Our activation energies, obtained by averaging these two values, are close to the charge-dependent values measured by several authors.[8,9]

In p-type material, no reaction involving Fe_i^+ and bond-centered hydrogen H_{BC}^+ is expected because of the long-range Coulomb repulsion. However, for moderate doping levels, the following reactions lead to pair formation:

$$^1Fe_i^0 + {}^{1/2}H_{BC}^0 \rightarrow {}^{1/2}\{Fe_i,H\}^0 + 0.82 \text{ eV}$$

and

$$^1Fe_i^0 + {}^0H_{BC}^+ \rightarrow {}^1\{Fe_i,H\}^+ + 0.40 \text{ eV}.$$

The $^{3/2}\{Fe_iH\}^0$ state is 0.26 eV (SIESTA) to 0.30 eV (VASP) higher than the $^{1/2}\{Fe_iH\}^0$ state. A second interstitial H will not bind to Fe_i. Indeed, the trigonal $\{Fe_iH_2\}^0$ complex (H-Fe-H, with Fe at the hexagonal interstitial site) is less stable by 0.45 eV than isolated Fe_i and an interstitial H_2 molecule.[103]

The interstitial $\{Fe_iH\}$ pair (Fig. 1) has trigonal symmetry. Fe is at the hexagonal interstitial site with Fe-H=1.51 Å. Figure 2 shows all the vibrational modes localized on Fe and H. The stretch mode frequency (1921 cm^{-1} with SIESTA, 1953 cm^{-1} with VASP) is higher than the 1767 cm^{-1} observed

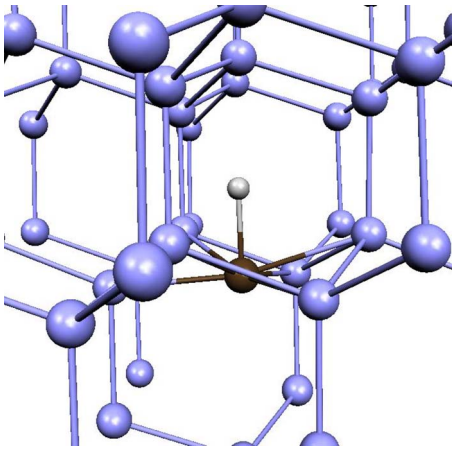

FIG. 1. (Color online) Fraction of the supercell showing the trigonal $^{1/2}\{Fe_iH\}^0$ pair. Fe (brown or dark grey sphere) is at the hexagonal interstitial site and H (small white sphere) is on the trigonal axis.

in free FeH molecules,[104] indicating that the interstitial pair is compressed by the host crystal.

The $\{Fe_iH\}$ pair has a deep donor and a deep acceptor level at $E_v+0.36$ eV (SIESTA: 0.42 eV) and $E_c-0.26$ eV (SIESTA: 0.30 eV), respectively. Thus, hydrogen has no passivating effect on Fe_i. In the contrary, the formation of the $\{Fe_iH\}$ pair results in the appearance of a new and deep acceptor level. A donor level at $E_v+0.31$ eV, believed to be associated with the interstitial $\{Fe_iH\}$ pair, has been reported by thermally stimulated capacitance.[69] This level anneals out in 30 min at 175 °C, suggesting a relatively weakly bound complex. This donor level and annealing behavior are consistent with the calculated donor level and binding energy. Note that two additional deep donor levels at $E_v+0.23$ eV and $E_v+0.38$ eV have been reported[105] following H implantation into Si samples contaminated with Fe. It is not known if these levels are related to isolated Fe_i or if native defects are involved.

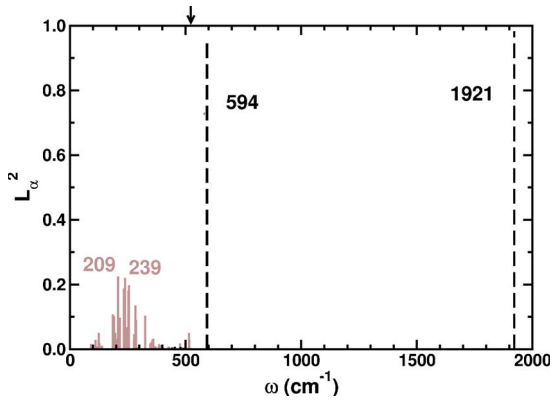

FIG. 2. (Color online) Vibrational spectrum of the interstitial $\{Fe_iH\}^0$ pair in Si. The short arrow shows the calculated Γ phonon. The plots show $L^2_{\{\alpha\}}=(e^s_{\alpha x})^2+(e^s_{\alpha y})^2+(e^s_{\alpha z})^2$, where α is Fe (solid brown or grey lines) or H (dashed black lines). The Fe-H stretch mode is at 1921 cm^{-1} and the (degenerate) wag modes are at 594 cm^{-1}.

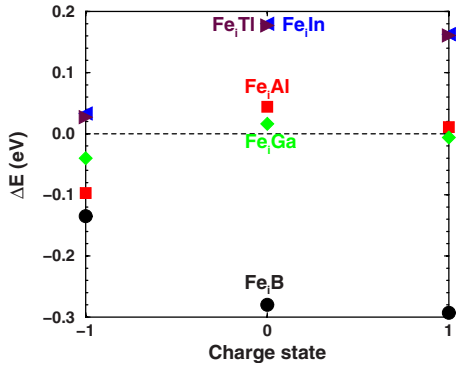

FIG. 3. (Color online) Calculated potential energy difference between the trigonal and orthorhombic configurations of the $\{Fe,A\}$ pairs, where A stands for B (black circle), Al (red square), Ga (green diamond), In (blue triangle left), and Tl (purple triangle right) in the three possible charge states of the pairs. ΔE is negative if the trigonal configuration is more stable.

B. Iron pairs with shallow dopants

1. Fe-acceptor pairs

We calculated the geometrical configurations, spin states, electronic structures, and binding energies resulting from the interactions of $^{3/2}Fe_i^+$ with the ionized shallow acceptors $^0A_s^-$, with A=B, Al, Ga, In, and Tl. $^{1/2}\{Fe,A\}^0$ is higher in energy than $^{3/2}\{Fe,A\}^0$ by several tenths of an eV. In the case of B for example, the energy difference is 0.42 eV with VASP and 0.41 eV with SIESTA.

We find two competing geometries for each $\{Fe,A\}$ pair: a trigonal configuration with Fe at (very near) one of the four T sites nearest to the acceptor, and an orthorhombic configuration with Fe at one of the twelve second-nearest T sites. Figure 3 shows the energy difference between the trigonal and the orthorhombic configurations in the three possible charge states, calculated a T=0 K. In this figure, ΔE is negative if the trigonal configuration is stable and the orthorhombic one metastable.

The free energy differences[102] between the trigonal and the orthorhombic configurations are plotted vs temperature in Fig. 4. In the present case, this involves only vibrational free energies since the difference in configurational entropy arising from the difference in the number of first- and second-nearest T sites can safely be ignored.[102] At room temperature, the predicted stable configurations match the experimentally-observed one in all cases.

Figure 5 shows the vibrational spectra of the $^{3/2}\{Fe,B\}^0$ pair in the C_{3v} and C_{2v} configurations. The isolated B_s^- acceptor has a threefold degenerate mode at 641 cm^{-1} (measured[106] at 620 cm^{-1}). In the {Fe,B} pair, the B-related line splits into a doublet and a singlet in C_{3v} symmetry, and three singlets in C_{2v} symmetry.

Previous calculations involving $\{Fe,A\}$ pairs have assumed that the shallow acceptor resides at an unrelaxed substitutional site and Fe at an undistorted nearest or second-nearest T site. Our geometry optimizations show that these assumptions are valid for Al, Ga, and In. All the ionized acceptors have tetrahedral symmetry and their four Si NNs

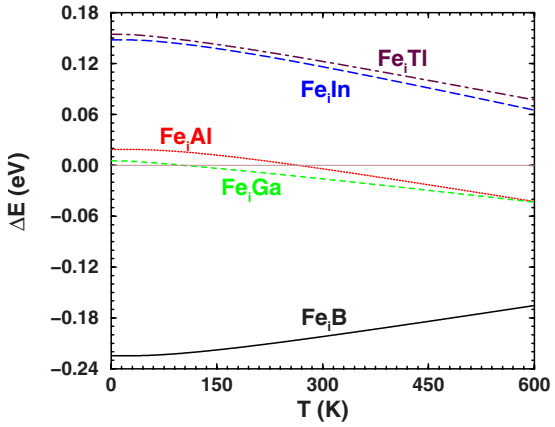

FIG. 4. (Color online) Calculated free energy differences between the trigonal and orthorhombic configurations of the $^{3/2}\{\mathrm{Fe},A\}^0$ pairs with A=B, Al, Ga, In, and Tl. ΔE is negative if the trigonal configuration is more stable.

are uniformly displaced inward (negative displacement) or outward (positive displacement) as follows: −0.27 Å for B_s^-, +0.05 Å for Al_s^-, +0.03 Å for Ga_s^-, +0.03 Å for In_s^-, and +0.16 Å for Tl_s^-. In the trigonal configuration, the Fe-acceptor separation is 2.35 Å for B (that is, Fe is exactly at the T site), 2.44 Å for Al, 2.44 Å for Ga, 2.44 Å for In, and 2.62 Å for Tl.

The binding energies of the neutral $\{\mathrm{Fe},A\}$ pairs were obtained by comparing the energies of each pair in its lowest-energy configuration to its dissociation products in different supercells: $^{3/2}\mathrm{Fe}_i^+ + {}^0A_s^- \rightarrow {}^{3/2}\{\mathrm{Fe},A\}^0 + E_b$. This energy balance has to be considered carefully since we are comparing the total energies of two supercells containing a charged defect (left-hand side) to the total energy of a neutral

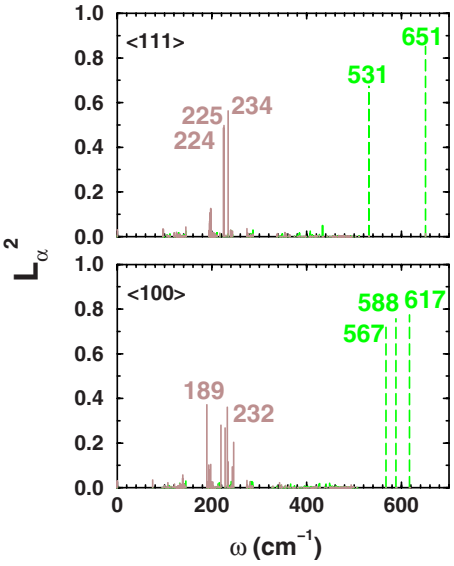

FIG. 5. (Color online) Vibrational spectra of the $^{3/2}\{\mathrm{Fe},\mathrm{B}\}^0$ pair in the trigonal and orthorhombic configurations. The plots show $L^2_{\{\alpha\}}=(e^s_{\alpha x})^2+(e^s_{\alpha y})^2+(e^s_{\alpha z})^2$, where α is Fe (solid brown lines) or B (dashed green lines)

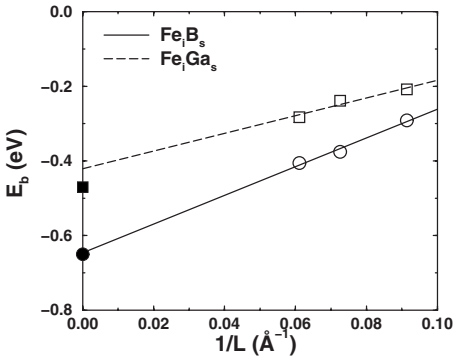

FIG. 6. Calculated binding energies of the neutral {Fe,B} (open circles) and {Fe,Ga} (open squares) pairs vs inverse supercell size. The solid circle and square are the measured binding energies.

pair. Hence, one needs to include Madelung energy corrections twice, but only on one side of the equation. Since the size of the correction diminishes as the size of the cell increases,[107] we repeated these calculations in cells containing 64 to 216 host atoms. Figure 6 shows the calculated binding energies of the {Fe,B} and {Fe,Ga} pairs vs inverse cell size (the binding energies of the other pairs look similar but crowd the figure).

The plots of binding energies vs. inverse cell size lead to the following calculated values for E_b extrapolated to infinite cell size: 0.65 eV for {Fe,B}, 0.52 eV for {Fe,Al}, 0.42 eV for {Fe,Ga}, 0.44 eV for {Fe,In}, and 0.55 eV for {Fe,Tl}. The experimental numbers (Table I in Ref. 1) are 0.45–0.65 eV for {Fe,B}, 0.52–0.70 eV for {Fe,Al}, and 0.47 eV for {Fe,Ga}. The experimental binding energies of {Fe,In} and {Fe,Tl} are not reported.

The origin of the binding energy is mostly Coulombic. The electrostatic energy gained by placing a +1 charge at 2.3–2.6 Å of a −1 charge in Si is of the order of 0.5 eV. However, as in the case of Cu-acceptor pairs,[108] the TM impurity does overlap weakly with the acceptor. Small differences in the Fe-A and Fe-$\mathrm{Si}_{\mathrm{NN}}$ overlap populations and small variations in the amount of lattice relaxation differentiate between the various acceptors.

The calculated donor and acceptor levels for the $\{\mathrm{Fe},A\}$ pairs in the two configurations are compared to the measured values in Table I.

Since interstitial hydrogen passivates[109] shallow acceptors such as B, we considered the possibility that the {Fe,B} pair may interact with H. Various *a priori* possible configurations for such a complex have been investigated. They include H bridging a B-Si bond or an adjacent Si-Si bond, H bound to Fe along or off the trigonal axis, or H at the Si antibonding site of a B-Si bonds.

The lowest-energy structure of the $^{3/2}\{\mathrm{Fe},\mathrm{B},\mathrm{H}\}^+$ complex has H bound to Fe in a trigonal Si-B$\cdots$Fe-H configuration. However, this complex is less stable than the dissociated species $^{3/2}\{\mathrm{Fe},\mathrm{B}\}^0$ and ${}^0\mathrm{H}^+_{\mathrm{BC}}$ by 0.07 eV. The minimum of the potential energy corresponds to Fe_i far away from the passivated {B,H} pair:

$$^{3/2}\{\mathrm{Fe},\mathrm{B}\}^0 + {}^0\mathrm{H}^+_{\mathrm{BC}} \rightarrow {}^{3/2}\mathrm{Fe}_i^+ + {}^0\{\mathrm{B},\mathrm{H}\}^0 + 0.25\ \mathrm{eV}.$$

TABLE I. Calculated (PAW) gap levels for the trigonal and orthorhombic configurations of {Fe,A} pairs with A=B, Al, Ga, In, and Tl. The donor (0/+) levels are given relative to the valence band: E_v+x (eV); the acceptor (−/0) levels are given relative to the conduction band: E_c-x (eV). When available, the experimental numbers are cited in parenthesis. All the references are in Sec. I.

	trigonal		orthorhombic	
A	E_v+x	E_c-x	E_v+x	E_c-x
B	0.11 (0.11)	0.29 (0.29)	0.11 (0.07)	0.45 (0.43)
Al	0.11 (0.20)	0.34	0.06 (0.13)	0.21
Ga	0.10 (0.24)	0.35	0.05 (0.14)	0.30
In	0.28 (0.27)	0.38 (0.32)	0.25 (0.15)	0.24 (0.39)
Tl	0.31	0.20	0.28	0.06

This suggest that H interacting with the {Fe,B} pair displaces Fe_i leaving the passivated {B,H} pair. This result has been inferred from DLTS measurements of hydrogenated samples.[110] The disappearance of the {Fe,B} DLTS peak following H implantation has also been reported by Kouketsu *et al.*[105] In this paper, the authors have interpreted the result in terms of H passivation of the pair. This interpretation is not supported by the calculated energetics.

2. Fe-donor interactions

In n-type Si, interstitial iron is the neutral $^1Fe_i^0$ species which experiences no Coulombic attraction to an ionized P^+ or As^+ shallow donor. The binding energy can only arise from changes in lattice relaxation and distortion, or covalent bonding between the two impurities. Since neither isolated Fe nor the isolated shallow acceptor are characterized by substantial atomic rearrangement in their immediate vicinity, one would not anticipate much elastic energy to be gained by pairing.

By analogy to the Fe-acceptor pairs, we have examined the trigonal and orthorhombic configurations for $^1\{Fe,D\}^+$ pairs (D=P or As), but find that no pair forms. Indeed, the reactions $^1Fe_i^0+{}^0D_s^+ \rightarrow {}^1\{Fe,D\}^+ + E_b$ give slightly negative binding energies in the 64 host atoms cells. Since comparable Madelung energy corrections occur on both sides of this equation, the binding energies should not vary much with cell size. Further, in this case, the free energy contributions will be dominated by a large configuration entropy term since there are orders of magnitude more T sites with Fe far away from the donor than adjacent to it.[102] This contribution to the free energy favors the dissociated species.

IV. SUMMARY AND DISCUSSION

First-principles theory is used to calculate the configurations, charge and spin states, electronic structures, binding and activation energies, and approximate acceptor and donor levels of isolated Fe_i, the {Fe_iH} pair, all the {Fe,A} pairs (A=B, Al, Ga, In, or Tl), and of Fe_i with D_s (D=P or As). The interactions between the {Fe,B} pair and H are also considered.

The host crystal is represented by periodic supercells containing 64 to 216 host atoms. The Kohn-Sham equations are solved within GGA with either plane-wave or pseudoatomic basis sets for the valence states. The geometries of the various defects in all the *a priori* possible spin and charge states are optimized using conjugate gradients with a $2\times2\times2$ k-point sampling. The location of the donor and acceptor levels are obtained with PAW potentials and a $3\times3\times3$ sampling using the marker method. The marker is the perfect crystal. The dynamical matrices are obtained using the force-constant approach at the Γ point. The vibrational spectra of the complexes involving light impurities are predicted. The free energy differences between the trigonal and orthorhombic configurations of the {Fe,A} pairs are calculated as a function of temperature.

The calculations predict that interstitial iron resides at the T site as $^{3/2}Fe_i^+$ or $^1Fe_i^0$, with a donor level at $E_v+0.28$ eV. There is no acceptor level. The spin density is localized on the TM impurity, with nearly 96% of the spin in the 3d orbitals of $^1Fe_i^0$, but only 78% in the case of $^{3/2}Fe_i^+$. The Fe atom overlaps weakly but covalently (positive overlap population) with its four nearest and six second-nearest Si neighbors. The activation energy for diffusion along the trigonal axis is 0.76 and 0.69 eV in the 0 and + charge state, respectively.

Fe_i traps interstitial H in the + and 0 charge states and forms a trigonal pair, with Fe at the hexagonal interstitial site. The binding energy relative to bond-centered hydrogen is 0.84 eV in the + charge state and 0.40 eV in the 0 charge state. The {Fe_iH} pair has a deep donor ($E_v+0.36$ eV) and a deep acceptor ($E_c-0.26$ eV) level in the gap. Thus, H does not passivate Fe_i but forms a pair which is even more electrically active.

The stable configuration of the {Fe,B} pair is trigonal, that of the {Fe,In} and {Fe,Tl} pairs is orthorhombic, and the two configurations are nearly degenerate in the case of the {Fe,Al} and {Fe,Ga} pairs. In each configuration, the pairs have a donor and a deep acceptor level. The calculated binding energies are close to the measured values. The binding of the pairs is mostly electrostatic in nature. If H is allowed to interact with the {Fe,B} pair, the lowest-energy configuration has a passivated {B,H} pair and isolated Fe_i. We find no pairing between Fe_i and the shallow donors P and As.

One of the key points of the present study is that first-principles theory in supercells, including conjugate gradient geometry optimizations, can be used to study the interactions of Fe in Si. The calculated properties of Fe_i and Fe-acceptor pairs are consistent with experiment: spin states, structures, energetics. The gap levels obtained with PAW potentials and the perfect crystal as a marker are close to the DLTS values. The calculated vibrational spectra of the {FeH} and {Fe,B} pairs predict several IR-or Raman-active LVMs.

Our best predictions for the donor and acceptor levels are obtained with PAW potentials and a $3\times3\times3$ k-point sampling in a 64 host-atoms supercell. The gap levels predicted with SIESTA are generally quite close to the PAW ones. The use of a uniform marker, the perfect cell, removes the "semi-empirical" aspect of the method, when different marker defects are used to scale the gap levels for different structures.

ACKNOWLEDGMENTS

This work of S.K.E. was supported in part by the National Renewable Energy Laboratory and the R.A. Welch Foundation Grant No. D-1126. The work of M.S. was supported by a grant from the Advanced Research Program of the State of Texas. Many thanks to Texas Tech's High Performance Computer Center for generous amounts of computer time.

*stefan.estreicher@ttu.edu

[1] A. A. Istratov, H. Hieslmair, and E. R. Weber, Appl. Phys. A **69**, 13 (1999).
[2] A. A. Istratov, H. Hieslmair, and E. R. Weber, Appl. Phys. A **70**, 489 (2000).
[3] H. H. Woodbury and G. W. Ludwig, Phys. Rev. **117**, 102 (1960).
[4] S. Greulich-Weber, J. R. Niklas, E. R. Weber, and J. M. Spaeth, Phys. Rev. B **30**, 6292 (1984).
[5] P. Schwalbach, S. Laubach, M. Hartick, E. Kankeleit, B. Keck, M. Menningen, and R. Sielemann Phys. Rev. Lett. **64**, 1274 (1990).
[6] G. Weyer, S. Degroote, M. Famciulli, V. N. Fedoseyev, G. Langouche, V. I. Mishin, A.-M. Van Bavel, A. Vantomme, and the ISOLDE Collaboration, Mater. Sci. Forum **258-263**, 437 (1997).
[7] U. Wahl, J. G. Correia, E. Rita, J. P. Araújo, J. C. Soares, and the ISOLDE Collaboration, Phys. Rev. B **72**, 014115 (2005); Nucl. Instrum. Methods Phys. Res. B **253**, 167 (2006).
[8] T. Heiser and A. Mesli, Appl. Phys. Lett. **58**, 2240 (1991); Phys. Rev. Lett. **68**, 978 (1992).
[9] H. Takahashi, M. Suezawa, and K. Sumino, Phys. Rev. B **46**, 1882 (1992).
[10] S. V. Koveshnikov and G. A. Rozgonyi, Appl. Phys. Lett. **66**, 860 (1995).
[11] T. Heiser and A. Mesli, Appl. Phys. Lett. **68**, 1868 (1996).
[12] D. Macdonald, T. Roth, P. N. K. Deenapanray, K. Bothe, P. Pohl, and J. Schmidt, J. Appl. Phys. **98**, 083509 (2005).
[13] C. B. Collins and R. O. Carlson, Phys. Rev. **108**, 1409 (1957).
[14] K. Wunstel and P. Wagner, Appl. Phys. A: Solids Surf. **27**, 207 (1982).
[15] K. Wunstel, K. H. Froehner, and P. Wagner, Physica B & C **116**, 301 (1983).
[16] V. B. Voronkov, A. A. Lebedev, A. T. Mamadalimov, B. M. Urunbaev, and T. A. Usmanov, Sov. Phys. Semicond. **14**, 1217 (1980).
[17] K. Nakashima and M. Chijiiwa, Jpn. J. Appl. Phys., Part 1 **25**, 234 (1986).
[18] O. O. Awadelkarim and B. Monemar, J. Appl. Phys. **64**, 6306 (1988).
[19] A. Rohatgi, J. A. Davis, R. H. Hopkins, P. Rai-Choudhur, and P. G. McMullin, Solid-State Electron. **23**, 415 (1980).
[20] H. Lemke, Phys. Status Solidi A **64**, 215 (1981).
[21] H. Feichtinger, J. Waltl, and A. Gschwandtner, Solid State Commun. **27**, 867 (1978).
[22] G. W. Ludwig and H. H. Woodbury, Phys. Rev. Lett. **5**, 98 (1960).
[23] G. Feher, Phys. Rev. **114**, 1219 (1959).
[24] A. L. Thilderkvist, G. Grossmann, M. Kleverman, and H. G. Grimmeiss, Phys. Rev. B **58**, 7723 (1998).
[25] H. Weihrich and H. Overhof, Phys. Rev. B **54**, 4680 (1996).
[26] G. W. Ludwig and H. H. Woodbury, in *Solid State Physics*, edited by F. Seitz and D. Turnbull (Academic, New York 1962), p. 223.
[27] W. Gehlhoff and U. Rehse, in *Defect Engineering in Semiconductor Growth, Processing, and Device Technology*, edited by S. Ashok, J. Chevallier, K. Sumino, and E. Weber (Materials Research Society, Pittsburgh, 1992), p. 507.
[28] J. M. Spaeth, S. Martini, and S. Greulich-Weber, Semicond. Sci. Technol. **13**, 725 (1998).
[29] H. Feichtinger, Inst. Phys. Conf. Ser. **46**, 528 (1979).
[30] S. D. Brotherton, P. Bradley, and A. Gill, J. Appl. Phys. **57**, 1941 (1985).
[31] X. Gao, H. Mollenkopf, and S. Yee, Appl. Phys. Lett. **59**, 2133 (1991).
[32] L. Dobaczewski, P. Kaminski, R. Kzlowski, and M. Surma, Mater. Sci. Forum **196-201**, 669 (1995).
[33] H. Nakashima, T. Sadoh, and T. Tsurushima, Phys. Rev. B **49**, 16983 (1994).
[34] S. Ghatnekar-Nilsson, M. Kleverman, P. Emaluelsson, and H. G. Grimmeiss, Semicond. Sci. Technol. **8**, 1857 (1993).
[35] S. Rein and S. W. Gluntz, J. Appl. Phys. **98**, 113711 (2005).
[36] H. Nakashima, T. Isobe, Y. Yamamoto, and K. Hashimoto, Jpn. J. Appl. Phys., Part 1 **27**, 1542 (1988).
[37] W. Wijaranakula, J. Electrochem. Soc. **140**, 275 (1993).
[38] H. Lemke, Phys. Status Solidi A **76**, 223 (1983).
[39] L. C. Kimmerling and J. L. Benton, Physica B & C **116**, 297 (1983).
[40] H. D. Mohring, J. Weber, and R. Sauer, Phys. Rev. B **30**, 894 (1984).
[41] J. J. van Kooten, G. A. Weller, and C. A. J. Ammerlaan, Phys. Rev. B **30**, 4564 (1984).
[42] W. Gehlhoff, K. Irmscher, and J. Kreissl, in *New Developments in Semiconductor Physics*, edited by G. Ferenczi and F. Beleznay (Springer, Berlin, 1998), p. 262.
[43] K. Irmscher, T. Kind, and W. Gehlhoff, Phys. Rev. B **49**, 7964 (1994).
[44] W. Gehlhoff, K. Irmscher, and U. Rehse, Mater. Sci. Forum **143-147**, 1233 (1994).
[45] W. Gehlhoff and K. Irmscher, Solid State Phenom. **32-33**, 219 (1993).
[46] A. Chantre and D. Bois, Phys. Rev. B **31**, 7979 (1985).
[47] H. Takahashi and M. Suezawa, Mater. Sci. Forum **258-263**, 443 (1997).
[48] G. W. Ludwig and H. H. Woodbury, Phys. Rev. **117**, 1286 (1960).
[49] W. Gehlhoff and U. Rehse, Solid State Phenom. **6-7**, 257 (1989).
[50] K. Wunstel, K. H. Froehner, and P. Wagner, Physica B & C **116**, 301 (1983).
[51] A. Chantre and L. C. Kimerling, Mater. Sci. Forum **10-12**, 387 (1986).
[52] W. Gehlhoff, P. Emanuelsson, P. Omling, and H. G. Grimmeiss, Phys. Rev. B **41**, 8560 (1990); Solid State Phenom. **19-20**, 207 (1991).

[53] W. Gehlhoff, P. Emanuelsson, P. Omling, and H. G. Grimmeiss, Phys. Rev. B **47**, 7025 (1993).
[54] P. Omling, P. Emanuelsson, and H. G. Grimmeiss, Mater. Sci. Forum **38-41**, 445 (1989).
[55] P. Omling, P. Emanuelsson, W. Gehlhoff, and H. G. Grimmeiss, Solid State Commun. **70**, 807 (1989).
[56] P. Emanuelsson, P. Omling, H. G. Grimmeiss, W. Gehlhoff, J. Kreissl, K. Irmscher, and U. Rehse, Mater. Sci. Forum **83-87**, 137 (1992).
[57] P. Tidlund, M. Kleverman, and H. G. Grimmeiss, Semicond. Sci. Technol. **11**, 748 (1996).
[58] M. Kleverman and P. Tidlund, Phys. Rev. B **56**, 15685 (1997).
[59] P. Tildund and M. Kleverman, Mater. Sci. Forum **258-263**, 455 (1997).
[60] T. E. Schlesinger and T. C. McGill, Phys. Rev. B **25**, 7850 (1982).
[61] R. Sauer and J. Weber, Physica B & C **116**, 195 (1983).
[62] S. P. Watkins and M. L. W. Thewalt, Can. J. Phys. **63**, 1074 (1985).
[63] H. Conzelmann, A. Hangleiter, and J. Weber, Phys. Status Solidi B **133**, 655 (1986).
[64] S. P. Watkins, M. L. W. Thewalt, and T. Steiner, Phys. Rev. B **29**, 5727 (1984).
[65] H. Takahashi, M. Suezawa, and K. Sumino, Mater. Sci. Forum **143-147**, 1257 (1994); and J. Appl. Phys. **78**, 3077 (1995).
[66] Y. H. Lee, R. L. Kleinhenz, and J. W. Corbett, Inst. Phys. Conf. Ser. **46**, 521 (1979).
[67] H. Overhof and H. Weihrich, Phys. Rev. B **55**, 10508 (1997).
[68] T. Mchedlidze and M. Suezawa, J. Phys.: Condens. Matter **16**, L79 (2004).
[69] T. Sadoh, K. Tsukamoto, A. Baba, D. Bai, A. Kenjo, T. Tsurushima, H. Mori, and H. Nakashima, J. Appl. Phys. **82**, 3828 (1997).
[70] G. G. DeLeo, G. D. Watkins, and W. Beall Fowler, Phys. Rev. B **23**, 1851 (1981); **25**, 4962 (1982); **25**, 4972 (1982).
[71] G. D. Watkins, G. G. DeLeo, and W. B. Fowler, Physica B & C **116**, 28 (1983).
[72] A. Zunger and U. Lindefelt, Phys. Rev. B **26**, 5989 (1982).
[73] A. Zunger, Phys. Rev. B **28**, 3628 (1983).
[74] H. Katayama-Yoshida and A. Zunger, Phys. Rev. Lett. **53**, 1256 (1984); Phys. Rev. B **31**, 7877 (1985).
[75] H. Katayama-Yoshida and A. Zunger, Phys. Rev. B **31**, 8317 (1985).
[76] A. Zunger, Solid State Phys. **39**, 275 (1986).
[77] F. Beeler, O. K. Andersen, and M. Scheffler, Phys. Rev. Lett. **55**, 1498 (1985); Phys. Rev. B **41**, 1603 (1990).
[78] L. V. C. Assali and J. R. Leite, Phys. Rev. B **36**, 1296 (1987).
[79] M. Sugimoto and A. Seki, Mater. Sci. Forum **196-201**, 1339 (1996).
[80] S. Zhao, L. V. C. Assali, J. F. Justo, G. H. Gilmer, and L. C. Kimerling, J. Appl. Phys. **90**, 2744 (2001).
[81] *Theory of Defects in Semiconductors*, edited by D. A. Drabold and S. K. Estreicher (Springer, Berlin, 2007).
[82] J. P. Goss, M. J. Shaw, and P. R. Briddon in *Theory of Defects in Semiconductors* (Ref. 81), p. 69.
[83] VASP 2003 at http://cms.mpi.univie.ac.at/vasp
[84] G. Kresse and J. Hafner, Phys. Rev. B **47**, 558 (1993).
[85] G. Kresse and J. Furthmüller, Phys. Rev. B **54**, 11169 (1996).
[86] G. Kresse and D. Joubert, Phys. Rev. B **59**, 1758 (1999).
[87] D. Sánchez-Portal, P. Ordejón, E. Artacho, and J. M. Soler, Int. J. Quantum Chem. **65**, 453 (1997).
[88] E. Artacho, D. Sánchez-Portal, P. Ordejón, A. García, and J. M. Soler, Phys. Status Solidi B **215**, 809 (1999).
[89] J. P. Perdew, *Electronic Structure of Solids '91*, edited by P. Ziesche and H. Eschring (Akademie Verlag, Berlin, 1991), p. 11.
[90] J. P. Perdew, K. Burke, and M. Ernzerhof, Phys. Rev. Lett. **77**, 3865 (1996).
[91] P. E. Blöchl, Phys. Rev. B **50**, 17953 (1994).
[92] H. J. Monkhorst and J. D. Pack, Phys. Rev. B **13**, 5188 (1976).
[93] D. Vanderbilt, Phys. Rev. B **41**, 7892 (1990).
[94] G. Kresse and J. Furthmüller, Comput. Mater. Sci. **6**, 15 (1996).
[95] N. Troullier and J. L. Martins, Phys. Rev. B **43**, 1993 (1991).
[96] O. F. Sankey and D. J. Niklewski, Phys. Rev. B **40**, 3979 (1989); O. F. Sankey, D. J. Niklewski, D. A. Drabold, and J. D. Dow, *ibid.* **41**, 12750 (1990).
[97] A. A. Demkov, J. Ortega, O. F. Sankey, and M. P. Grumbach, Phys. Rev. B **52**, 1618 (1995).
[98] J. Izquierdo, A. Vega, L. C. Balbás, D. Sánchez-Portal, J. Junquera, E. Artacho, J. M. Soler, and P. Ordejón, Phys. Rev. B **61**, 13639 (2000).
[99] V. M. García-Suárez, C. M. Newman, C. J. Lambert, J. M. Pruneda, and J. Ferrer, J. Phys.: Condens. Matter **16**, 5453 (2004).
[100] V. L. Moruzzi and C. B. Sommers, *Calculated Electronic Properties of Ordered Alloys: A Handbook* (World Scientific, Singapore, 1995).
[101] S. K. Estreicher, D. West, J. Goss, S. Knack, and J. Weber, Phys. Rev. Lett. **90**, 035504 (2003).
[102] S. K. Estreicher, M. Sanati, D. West, and F. Ruymgaart, Phys. Rev. B **70**, 125209 (2004).
[103] S. K. Estreicher, Acta Phys. Pol. A **102**, 403 (2002).
[104] G. V. Chertihin and L. Andrews, J. Phys. Chem. **99**, 12131 (1995).
[105] M. Kouketsu, K. Watanabe, and S. Isomae, Mater. Sci. Forum **196-201**, 861 (1995).
[106] C. P. Herrero, M. Stutzmann, and A. Breitschwerdt, Phys. Rev. B **43**, 1555 (1991).
[107] J. Lento, J.-L. Mozos, and R. M. Nieminen, J. Phys.: Condens. Matter **14**, 2637 (2002).
[108] S. K. Estreicher, Phys. Rev. B **60**, 5375 (1999).
[109] S. K. Estreicher, Mater. Sci. Eng., R. **14**, 319 (1995).
[110] O. V. Feklisova, A. L. Parakhonsky, E. B. Yakimov, and J. Weber, Mater. Sci. Eng., B **71**, 268 (2000).